Hawaiian Basalt Characterization and the Effects of Chemical Composition Variances on the Sintering Process; Potential Implications for Lunar/Mars ISRU Applications.

Kyla Edison [a]*, Christian Andersen[a], Kye Harford[a], Kylie Higaki[b], Rodrigo Romo[a]

[a] The Pacific International Space Center for Exploration Systems (PISCES), 99 Aupuni St. Suite 212-213, Hilo, HI 96720, deforeky@hawaii.edu, canderse@hawaii.edu, kharford@hawaii.edu, rfvromo@gmail.com

[b] Oregon State University, Oregon State University, 104 Kerr Admin Building, Corvallis, Oregon 97331, kyliehigaki@gmail.com

**Corresponding Author*

Abstract

In Situ Resource Utilization (ISRU) refers to the ability to utilize local resources found in an area of interest. In space exploration and settlement, ISRU aims to utilize resources found on the moon and Mars to build infrastructure, thereby reducing the need for materials from Earth. Consequently, there is a high degree of interest in lunar and Mars regolith as a source for construction materials and volatiles extraction.

Sintering is one proposed method to produce a manufacturing and/or construction material feedstock using lunar and Martian regolith. The Pacific International Space Center for Exploration Systems (PISCES) in collaboration with NASA's SwampWorks successfully developed interlocking tiles made with sintered basalt from a quarry on the island of Hawai'i. Hawai'i's basalt has chemical properties similar to those of lunar and Martian regolith. PISCES has developed sintered materials under two different thermal profiles (1,149 °C & 1,177 °C) using basalt feedstock. The structural properties of this material exceeded the strength of both residential and specialty concrete.

PISCES has continued researching basalt sintering since its project with SwampWorks, characterizing basalt samples from multiple locations on Hawai'i island. Chemical analyses have revealed a significant variation in composition among basalts based on their source, age and flow they originated from. These samples were sintered using the two aforementioned temperature profiles to determine how their varying chemical compositions affect the resulting product. The results show that chemical composition plays a significant role in the quality of the final sintered material. While some samples produce exceptionally durable blocks, others result in materials that would not function well for manufacturing or construction.

Identifying desirable basalt characteristics for sintering will aid in the search for locations and sources of optimal basalt regolith for sintering on the moon and Mars. Moving forward, thin section analysis, X-Ray Diffraction (XRD) and more structural testing is needed to better characterize the relationship between regolith composition and sintering quality.

Keyword: ISRU, Sintering, Basalt, Chemical composition, Mineralogical Composition, Olivine Porphyries

1. Introduction

PISCES is a state-funded aerospace agency located in Hilo, Hawai‘i that has been investigating ways to use regolith to create construction materials applicable to ISRU on the moon and Mars. Basalt is a fine-grained volcanic rock containing 45-52 % silica and is composed largely of plagioclase, pyroxene and olivine. This is not to be confused with Ultramafic rocks which contain <45 % silica and largely containing olivine. Basalt is the most abundant rock found on Earth, the moon and Mars. Depending on its age, location and volcano of origin, basalt's chemical composition and mineral abundances can vary.

The similarity of basalts found on different terrestrial planets has prompted research to use it as a construction feedstock material, sparing the costly expense of transporting such materials from Earth. Creating construction materials from lunar/Martian regolith will be vital for future settlements to protect humans from radiation, mitigate dust, provide thermal insulation and support infrastructure.

One method to convert basalt into a manufacturing feedstock is through sintering. Sintering is a thermal process used to bond contacting particles into a solid object [4]. Due to basalt's varying compositions, it is important to test their sintering properties .

Since 2014, PISCES has researched high temperature sintering with Hawaiian to create construction materials applicable to lunar/Martian ISRU. Hawai‘i basalts were selected for this research due to their wide availability in Hawai‘i, and their geochemical likeness to lunar and Martian regolith [16]. In the past, Hawaiian basalt aggregate has also been used in the Martian regolith simulant JSC MARS-1 [1].

In 2016, PISCES teamed up with NASA's SwampWorks under the Additive Construction with Mobile Emplacement (ACME) project to create sintered basalt pavers for a vertical launch and landing pad. The launch pad was submitted to a static rocket motor test [10]. While the tiles showed some design weaknesses, the sintered material showed no degradation from the high temperature and velocity of the motor's exhaust. The results from this test set the path to further develop the sintering process and the evaluation of the effect that chemical composition has on the sintered material.

2. Methods

2.1 Characterization

The basalt used in the sintered tiles for the ACME project was obtained from a Hawai‘i Island quarry. However, the island has many lava flows and quarries containing basalt with varying chemical compositions. A geologic map overlay with Google Earth Pro [3] was used to determine a basaltic lava flow's location, volcano of origin, age and magma series (chemical composition of magma).

Basalt samples were collected from local commercial quarries and three lunar/Martian analogue sites. These sites are recognized by

NASA [11] as being analogous to the moon and Mars and have been used for planetary research since the Apollo program.

2.1.1 Energy Dispersive X-Ray Fluorescence (EDXRF)

The collected samples were analyzed using Energy Dispersive X-Ray Fluorescence (EDXRF) at the University of Hawai‘i at Hilo Geology department. Each sample was powdered using a shatter box and compressed into a pellet using a pellet press.

2.1.2 Feedstock mineralogy

According to *Advanced Automation for Space Missions (1982)* [2], raw feedstock basalt should contain pyroxene $(Ca, Mg, Fe)SiO_3$ in excess of 60% (for casting basalts). This mineral imparts qualities such as resistance to abrasion, mechanical strength and chemical resistivity. The minerals magnetite (Fe_3O_4) and olivine $(Mg, Fe)_2SiO_4$ promote crystallization within the casted mass. Olivine content must not exceed 10% due to its high melting point and its potential to burst during the annealing process. Feldspars (plagioclase) $(Na, Ca)Al_{1-2}Si_{3-2}O_8$ tend to influence viscosity and regulate the rate of crystallization [2].

Each sample was examined under a binocular microscope to assess its mineralogy and visible mineral content. This provided the starting point which lead to more in-depth testing using X-Ray Diffraction (XRD).

2.1.3 X-Ray Diffraction (XRD)

Using a TERRA Mobile XRD System [6] from the University of Hawai‘i at Mānoa’s Department of Earth Science, a qualitative crystal analysis was conducted on each sample. Samples were sieved at 150 μm. Each 15mg sample was scanned 3 to 6 times for accuracy.

Data gathered from the CheMin instrument aboard NASA’s Curiosity rover on Mars was also used to compare it to the Hawaiian basalt mineralogy. Lunar data has not been obtained at this time but will be in the future [13].

3. Sintering

All basalt samples were dried in a kiln for 12 hours at 121 °C and placed into a ceramic mold, lightly compressed and sintered. For the purpose of this paper, only two sintering thermal profiles were evaluated: 1,149 °C and 1,177 °C. Testing shows that sintering at temperatures below 1,149 °C does not result in particle bonding. At higher temperatures, the basalt becomes more fluid and tends to crystallize into the molds via pores, making it more difficult to work with.

Due to basalt’s variations of mafic mineral abundances—the most common being plagioclase, olivine and pyroxene, all having different melting temperatures—its melting point varies, resulting in a range. To understand this range, a phase diagram was used (see Fig. 1) [15]. Though this graph is typically used for mantle melting (rich in olivine) and does not provide an exact reference for this type of melt, it does give a relative idea of the melting range for basalt. Typically, when discussing mantle melting, there is a relation of chemical composition, depth and high temperatures. For this project, basalt is being fired at one atmosphere of

pressure and high temperatures to test how its chemical composition affects sinterability, taking depth out of consideration.

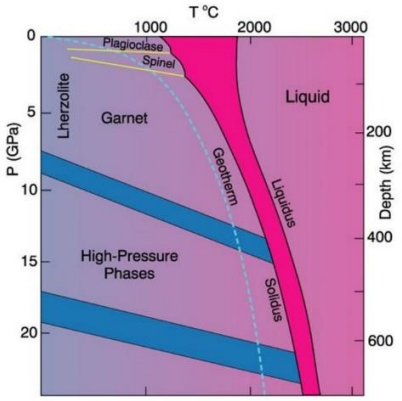

Fig. 1 Phase diagram of aluminous lherzolite with melting interval, sub-solidus reactions and geothermal gradient eutectic.

To use this graph effectively, one must consider melting basalt at atmospheric pressure; 0 GPa was assumed (1 Atm = 0.000101325 GPa). To check the graph's applicability, a sample was sintered at 1,065 °C (at solidus). Sintering did not occur at this temperature but started at 1,120 °C (just past the solidus). More heat was needed to gain a quality sintered product. The profiles of 1,149 °C & 1,177 °C seem to be the ideal temperature range to produce a quality sintered material at one atmosphere of pressure.

3.1 Sintered materials thin sections

Thin section analysis was taken from sintered samples that yielded exceptional quality to observe their crystal behavior. Thin sections were made by Wagner Petrographic [14] and impregnated with blue epoxy to bring out the pores (distinguish between glass/crystal/pore). One sample of poor sintering quality was also cut to compare with the quality materials. In the future, thin sections of all sintered materials and their parent rocks will be analyzed for comparison and to track changes in their crystalline structure.

4. *Structural testing*

4.1 Density

Sintered samples were subjected to a variety of tests including density, absorbency (general porosity), flexural and compressive strength analysis. A laboratory scale was used to test the samples mass. Then a simple volume was calculated using the equation ρ=m/v to solve for density.

4.1.2 Absorbency

Absorbency was tested to gain a general idea of porosity. The testing was conducted by calculating the mass of dry sintered samples, then submerging them in water for 24 hours. Samples were removed from the water and then weighed while they were saturated. The difference between saturated and dry mass was recorded. To calculate the amount of water absorbed by the sintered sample the following equation was used:

$(M_2 - M_1)/v * 100$ (1)

Where:

M_1 = dry mass

M_2 = saturated mass

v = volume of sintered material

4.1.3 Flexural and compressive strength

Flexural and compressive strength testing was conducted on both first-generation sintered products (2016). These materials were tested by NASA's Kennedy Space Center, conducted in accordance with ASTM

C133, Standard Test Methods for Cold Crushing Strength and Modulus of Rupture of Refractories. At the time, it was only possible to test samples fired at 1,149 °C and one sample of 1,177 °C. Both samples were from Quarry 1 (at the time this was the only material collected).

Second-generation materials (2017) were tested by the University of Hawai‘i at Mānoa. Like the first-generation, the materials were tested in accordance to ASTM C133. In 2017, only materials fired at 1,149 °C were tested because the process to fire at 1,177 °C was still under development. This test included feedstocks from other commercial quarry sites. Analogue sites were not included in these tests because they were not collected at this time. Testing for all sintered materials from all sample locations fired at both 1,149 °C and 1,177 °C will take place soon.

5. Results

5.1 Characterization

Fig. 2 Displays the USGS Google Earth Pro map overlay where samples were collected, their lava flow and volcano of origin.

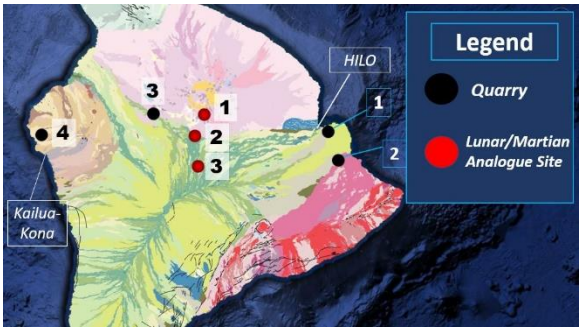

Fig. 2 USGS geologic map overlay of the island of Hawai‘i and sample locations.

5.1.2 Energy Dispersive X-Ray Fluorescence (EDXRF)

The EDXRF was plotted into the International Union of Geological Sciences (IUGS) rock classification for igneous rocks graph. This graph is a helpful tool identifying aggregate rock types based on their chemical composition. Data from the moon and Mars were also plotted into the graph and compared to Hawaiian basalt aggregates feedstock (see Fig. A2 in Appendix).

5.1.3 Feedstock mineralogy

Imagery of the quarry aggregate under binocular microscope reveals that Quarry 2B and 4 have a high percentage of large olivine phenocrysts. While samples Quarry 1 and 3 seem to have some olivine, however the crystals are smaller and seem to make up a lower percentage of the feedstock’s mineral abundances (see Fig. 3).

The analogue sites in Hawai‘i are not true basalt, but predominantly made up of basalt scoria or tephra. Scoria forms when dissolved gas flows from a volcano or is blown out during an eruption. It is made up of fragmented crystals and a high percentage of volcanic glass [15].

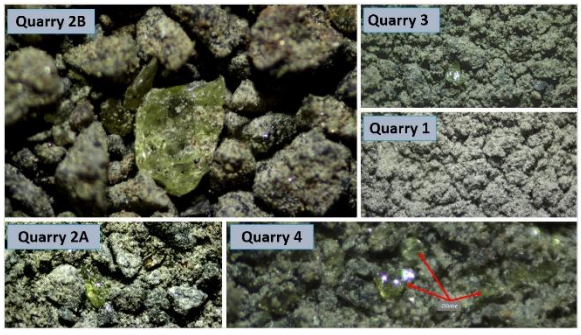

Fig. 3 Hawaiian basalt aggregate under binocular microscope.

Tephra is mostly ash and rock fragments from an eruption. Fig. 4 below show almost

no visible crystals and a highly vesiculated oxidized grain mass for all the analogue samples.

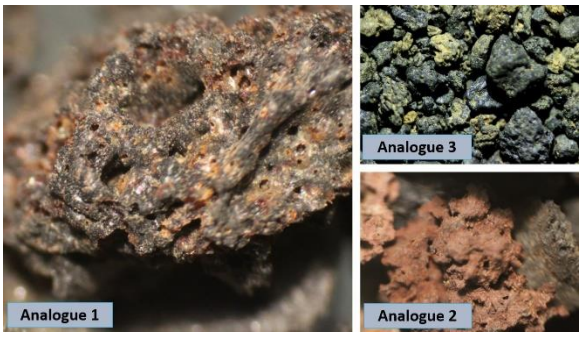

Fig. 4 Analogue site feedstock under binocular microscope.

5.1.4 X-ray Diffraction Analysis

Fig. A3 can be found in the Appendix and displays the XRD results for all Hawaiian aggregate samples collected thus far.

Fig. A4 can be found in the Appendix and includes XRD data collected from the CheMin database. It will be used to compare against the Hawaii samples [13].

6. Sintering

Of the five samples from local quarries, Quarry 1 and Quarry 3 produced the most cohesive sinter at both temperature profiles. Quarry 2B sintered so poorly that the basalt grains were easily brushed off from the material and could be broken by hand. Due to the poor nature of its sinter, Quarry 2B was not submitted for structural testing. Quarry 4 also sintered poorly, but better than 2B. Quarry 4 was tested to gauge its structural integrity and compare against Quarry 1 and 3. At first glance, Quarry 2A did not have a successful sinter. Upon further inspection of the material, only certain spots of the material did not sinter. Other spots appeared to sinter as well as Quarry 1 and 3. Fig. 5 displays Quarry samples sintered at 1,149 ℃. Fig. 6 displays materials sintered at 1,177 ℃. Quarry 2A and B have only been sintered at 1,149 ℃ due to limited feedstock.

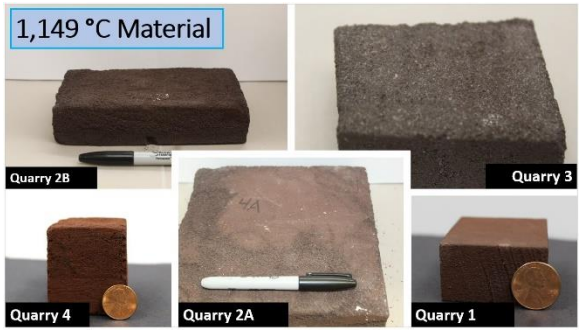

Fig. 5 All Quarry samples sintered at 1,149 ℃.

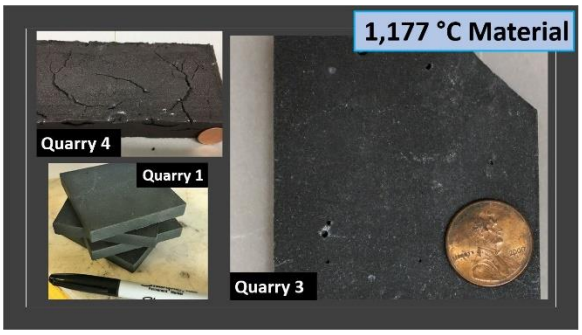

Fig. 6 All samples except Quarry 2 sintered at 1,177 ℃.

The analogue site samples did not sinter well at the above temperature profiles. The temperature needed to be lowered due to the samples coming out vitrified, shrunken and burnt (see Fig. 7).

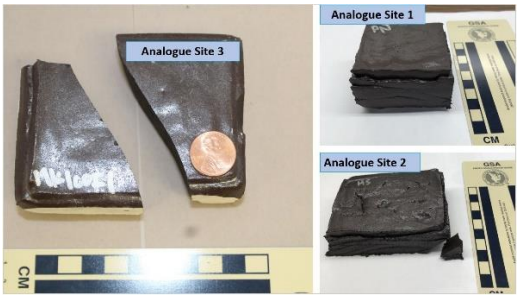

Fig. 7 Analogue sites sintered at 1,149 ℃.

Only Analogue 1 was used in the low temperature firing due to the abundance of feedstock available for use. Analogue 1 is close enough in composition to Analogue 2 that the results should be very similar. More testing needs to be conducted on Analogue 3. However, feedstock for this sample is difficult to obtain. To find the best sintering temperature for the analogue sites, the lowest possible temperature was selected. The feedstock was fired to the highest possible temperature (when they began to shrink and vitrify). At 1,066 °C, the sample did not sinter. This was expected due to the temperature sitting at solidus. For each bake, the temperature was raised incrementally until the samples began to look vitrified and burnt. At 1,121 °C, the material created resembled the sintered material created from Quarry 1 and 3 at 1,149 °C. The temperature was then increased to 1,135 °C, resulting in a material similar to Quarries 1 and 3 (see Fig. 8). Firing at 1,121 °C produced an oxidized and porous material; firing at 1,135 °C caused slumping and vitrification. Temperatures exceeding 1,135 °C created vitrified and burnt material.

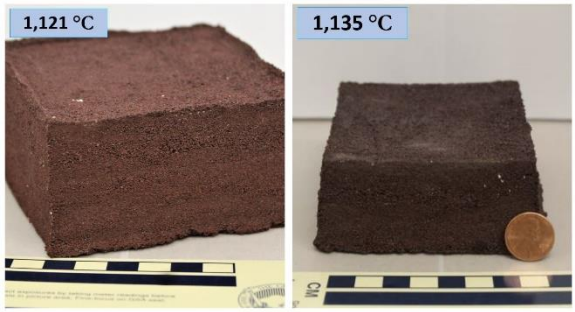

Fig. 8 Analogue 1 sintered at 1,121 °C (left) and 1,135 °C (right).

6.1 Sintered material thin sections

Thin sections were taken from sintered samples from Quarries 1, 3 and 4 that were fired at 1,149 °C. However, material fired at 1,177 °C was only cut from Quarries 1 and 3. Quarries 1 and 3 had exceptional sinterability and needed testing to compare their mineralogy. Quarry 4 was selected because it was an exceptionally poor sinter. To investigate how mineral abundances affected sinterability of a feedstock, Quarry 4 was used to compare with Quarries 1 and 3.

Results of this analysis showed that for all thin sections, there was a heavy percentage of pore space. The materials sintered at 1,149 °C have more pores than the materials fired at 1,177 °C. This is typical of the sintering process. The higher the temperature, the more fusion between grains [4].

7. Structural Testing

7.1 Density

Table 1 shows the measurements and densities of all samples tested.

Sintering Temperature	Sample	Density (g/cm^3)
1,149 °C	Quarry 1	*2.21*
	Quarry 2A	*N/A*
	Quarry 2B	*N/A*
	Quarry 3	*2.39*
	Quarry 4	*1.4*
	Analogue 1	*2.53*
	Analogue 2	*2.33*
	Analogue 3	*2.39*
1,177 °C	Quarry 1	*2.61*
	Quarry 3	*2.58*
	Quarry 4	*2.09*
1,121 °C	Analogue 1	*1.52*
1,135 °C	Analogue 1	*1.82*

Table 1. Density results for all samples sintered at all thermal profiles.

7.1.2 Absorbency

Results for the absorbency tests are shown in Table 2.

Sintering Temperature	Sample	Absorbency %
1,149 °C	Quarry 1	*12.07*
	Quarry 2A	*N/A*
	Quarry 2B	*N/A*
	Quarry 3	*30.92*
	Quarry 4	*41.02*
	Analogue 1	*1.49*
	Analogue 2	*1.09*
	Analogue 3	*1*
1,177 °C	Quarry 1	*2.65*
	Quarry 3	*3.27*
	Quarry 4	*23.7*
1,121 °C	Analogue 1	*35.72*
1,135 °C	Analogue 1	*19.24*

Table 2. Absorbency test results for all samples collected and sintered at all current thermal profiles.

7.1.3 Flexural and compressive strength testing

In 2016, structural tests were conducted for sintered material feedstock from Quarry 1 for materials fired at 1,149 °C & 1,177 °C. Results of this test are shown in Fig. 9. The 2017 structural tests were only those that were fired at 1,149 °C. However, sintered materials from a variety of locations on Hawai‘i Island were tested (see Fig. 10). During this time, the thermal profile and ramp times for the 1,177 °C profile was being developed and no samples were available for testing. Structural tests for all samples fired at 1,177 °C will be conducted soon.

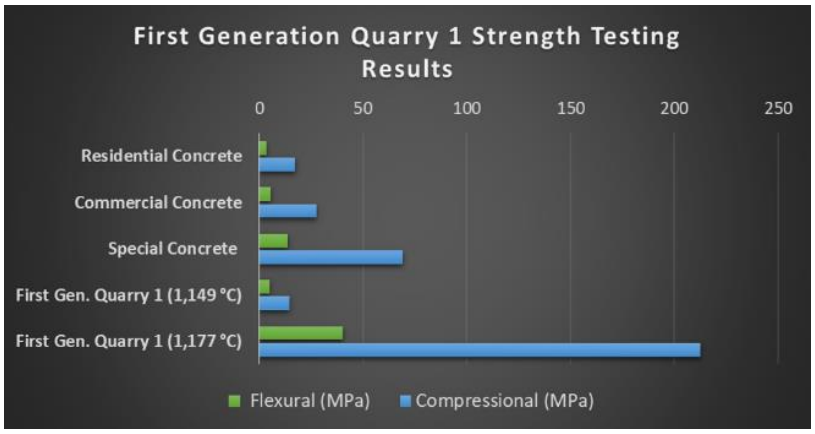

Fig. 9 First-generation structural testing for flexural and compressive strength Quarry 1. This includes samples fired at 1,149 °C and 1,179 °C.

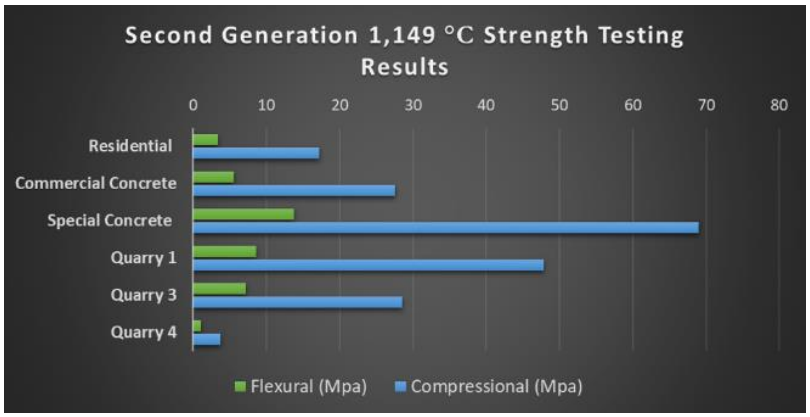

Fig. 10 Second-generation flexural and compressive strength testing for all samples fired at 1,149 °C.

8. Discussion

Fig. A1 and Table 3 in the Appendix display the EDXRF results for all Hawaiian aggregate samples, Martian and Lunar samples. The Hawaiian feedstock results show a slight spike in MgO % for Quarry 2A and a significant spike in MgO % for samples from Quarry 2B and Quarry 4. It was hypothesized that this is due to an abundance of forsterite olivine (Fo). Fo is the magnesium endmember in the olivine group $(Mg_2)SiO_4$ and its melting temperature is 1,890 °C—a much higher temperature than the current sintering thermal profiles being

used. The EDXRF revealed a striking chemical similarity between the Hawaiian aggregate, and both the moon and Mars. Both the moon and Mars have a higher percentage of FeO %, while the moon has a higher percentage of Al_2O_3 than Hawaiian basalts.

The data points from the IUGS Classification of Igneous Rocks graph show that the Lunar EDXRF data points tend to be concentrated between the picrobasalt and tholeiitic basalt range. Hawai‘i and Mars were more densely concentrated between tholeiite and basaltic andesite, displaying the similarities between Hawaiian and Martian basalts clearly. Picrobasalt is also common in Hawai‘i, but coincidentally none of the collected samples fell within that category [9]. In the future, Hawaiian picrite will also be tested for sinterability. The Analogue 1 & 2 samples are all predominantly made of volcanic glass and plagioclase, falling in line with the definition of basalt scoria. In the case of Analogue 3, plagioclase and glass are dominant. Results for the mineral and chemical compositions all match with their classification in the IUGS igneous rock classification graph.

It is thought that the structurally weak materials were abundant in Fo. Observing the feedstocks using a microscope showed that Quarry 1 and 3 samples had small Fo crystals. However, XRD measurements to determine the actual weight percentage of crystals found within each sample revealed Fo olivine to be 0%. Both Quarries 1 and 3 are both dominated by plagioclase and pyroxene. Samples from Quarry 2B and Quarry 4 both have an abundance of porphyritic Fo that shows up as 33.6%, a substantial amount compared to the rest of the mineral abundances.

Quarries 1 and 3 had the most cohesive and durable sinter of all the samples collected. The XRD data showed that both samples have an abundance of plagioclase ranging from 42.7% for Quarry 1 and 46.4% for Quarry 3. The XRD data shows no olivine present in the two samples. Quarry 4 has an abundance of olivine at 33.6% and a much lower percentage of plagioclase (27.1%) than Quarry 1 and 3. The sinter was poor for Quarry 4 and it has been observed that the large olivine crystals are acting as a void between grains. Sintering works by fusing uniform grains to one another to form a solid mass. If olivine is not melting and fusing with the other grains, then the entire mass will fail.

Due to the amount of volcanic glass found at the analogue sites, the samples were found to sinter at a much lower temperature than the true basalt aggregates. It is believed that the glass is melting more readily than the minerals. This has implications for energy saving if sintering is applied on the moon and Mars. Results for both types of basalt aggregate feedstock and basalt scoria highlight that chemical and mineral composition play a significant role in sinterability. There appears to be a “recipe” to form the best sintered material. According to *Advanced Automation for Space Missions (1982)*, raw feedstock basalt should contain pyroxene $(Ca, Mg, Fe)SiO_3$ in excess of 60% (for casting basalts). It is an important mineral to have as it imparts qualities such as resistance to abrasion, mechanical strength, and chemical resistivity. The minerals magnetite $(Fe)_3O_4$ and olivine Mg_2SiO_4 are important as they promote crystallization

within the casted mass. Olivine must not exceed 10% as it doesn't melt readily, causing bursting during the annealing process. Feldspars (plagioclase) $(Na, Ca)Al_{1-2}Si_{3-2}O_8$ tend to influence viscosity and regulate the rate of crystallization [2].

The data shows that when sintering basalt, it is desirable to have an abundance of plagioclase as opposed to pyroxene. Fo olivine porphyries have a negative impact on the structural integrity, forming weak spots within the body of the material. Glass in abundance allows for a lower temperature sinter, possibly due to the readiness of glass to melt compared to crystals. However, structural testing is needed to check its viability as a material. Clearly there is an ideal ratio between minerals and glass to create the most durable materials. More testing is required to definitively identify that ratio. However, it appears that an abundance of plagioclase, low olivine and moderate glass content creates a structurally durable material.

This conclusion is supported by the thin section analysis. Immediately, it is noticeable that in all thin sections there is a dense population of large blackened crystals wedged within the matrix of sintered material. Typically, a thin section of igneous rock would indicate that these crystals are an opaque volcanic glass. But the Fo olivine was not apparent. This was concerning because the feedstock and XRD analysis revealed olivine in the samples, but they did not readily appear in the thin sections. Upon further analysis, it was found that the blackened crystals must be the Fo olivine and possibly some pyroxene. Further inspection under polarized light showed remnants of third order colors and faint conchoidal fracture (identifiers of Fo olivine). It is suspected that olivine is the least stable mineral at higher temperatures, breaking down and ejecting Fe and resulting in a purer form of Mg olivine. This completely converts and oxidizes the olivine, leaving it blackened. SEM analysis and more research will be needed to confirm if this is the Fo olivine, and to support the above claim. Fig. 11 and 12 show examples of the remnant third order colors and conchoidal fracture.

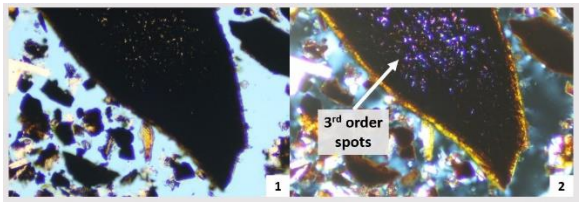

Fig. 11 White light (left) blackened crystal assumed to be olivine. Polarized light (right) displaying possible 3rd order birefringence peeking through the crystal.

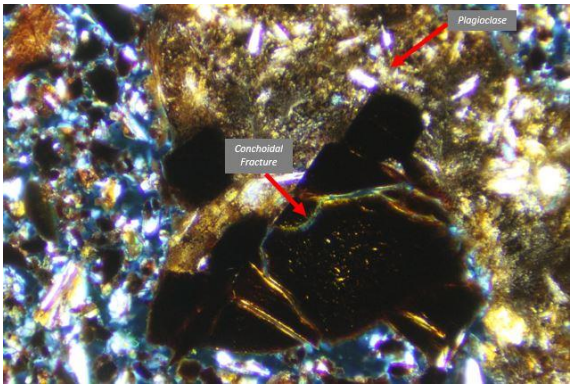

Fig.12 Blackened crystal under polarized light showing conchoidal fracture and remnant 3rd order birefringence not yet affected by sintering.

The first-generation structural testing of Quarry 1 showed that when fired at 1,149 °C, the material produced has a ~2x greater

flexural and compressive strength than residential concrete. When the same sample feedstock was fired at 1,179 °C, the material produced had ~3x greater flexural and compressive strength than specialty concrete. When observed under a microscope it is easy to see that the 1,149 °C material has a greater amount of pore space compared to the 1,177 °C material. As a higher thermal profile is applied, pore space closes between grains creating a more structurally sound material.

Second-generation materials included samples from the four Quarries but did not include analogue sites or materials fired at 1,177 °C. Results of this test align with the idea that Fo olivine porphyries may affect a material's sinterability significantly. The feedstocks that yielded a poor sinter were Quarries 2B and 4—both with a much higher percentage of olivine than the other samples. To continue testing this idea, picrite basalt (olivine basalt) has been collected and will be tested for sinterability. It is hypothesized that it will not sinter well at any of the current thermal profiles. More research in mineralogy and structural testing of all samples sintered thus far is needed to further investigate the ideal recipe for basalt sintering.

9. Conclusion

The results of this research have clearly indicated that chemical composition and mineral abundances—particularly Fo olivine porphyries—play a significant role in sinterability. High plagioclase, low olivine and moderate glass content tend to yield a structurally durable material when fired at 1,149 °C and 1,179 °C. A high abundance of olivine porphyries, moderate pyroxene and low glass tend to produce a poorly sintered, non-cohesive material. Samples that are predominantly made up of volcanic glass reduce the necessary temperature for sintering, ultimately reducing the energy needed.

Future studies in this area will include the possibility of sintering with a high-percentage olivine feedstock. This will be done by adding a higher percentage of glass to act as a binder between the large olivine porphyries and other grains. This research could have implications for mining regolith on the moon and Mars, eliminating the need to find an absolute chemical composition to achieve coherent sintering. Even so, data indicates there may be areas of the moon and Mars where the ideal chemical composition of regolith needed for sintering is present. Based on EDXRF and XRD data, Martian regolith is strikingly similar to Hawai‘i basalts. Martian samples that may yield an exceptional sinter come from the CheMin data gathered by the Curiosity rover. These include Telegraph Peak and Confidence Hill located in Gale Crater (so long as there are no Fo porphyries). Due to a lack of mineral data, it is unclear if Mars Pathfinder samples will work. However, according to the EDXRF data they match up closely to the Hawaiian aggregates that sintered well.

The Lunar regolith data is based on EDXRF results and shows that chemically, those samples are more concentrated in the picrobasalt category. This may result in exceptionally poor sintering due to the presence of picrites and porphyritic Fo crystals. Predictions for the moon are

difficult with limited EDXRF and XRD data currently available.

Future work will include more research on the effect that Fo olivine has on the sintering process, and whether the use of binders or the addition of a higher percentage of glass may mitigate them. Since chemical composition and mineral abundances appear to play a significant role in sinterability, the next steps in research would include vacuum sintering with the same processes outlined in this paper. Mineralogy testing like SEM and more thin section analysis is also needed, as well as structural analysis for all samples sintered so far.

Acknowledgments

Mahalo to the PISCES team for their dedication and support to this project, and to the interns for their hard work. Special Mahalo to Ken Hon for providing the IUGS graph skeleton and mineralogy assistance, Jeff Taylor for loaning the Terra XRD and his enthusiastic support, and to Steve Lundblad for allowing the team to work in the Geology lab at UH Hilo and for running the EDXRF samples. Mahalo Nui Loa to everyone who made this project possible.

References

[1] Allen, C. C., Morris, R. V., Jager, K. M., Golden, D. C., Lindstrom, D. J., Lindstrom, M. M., & Lockwood, J. P. (1998, March). Martian regolith simulant JSC Mars-1. In Lunar and planetary science conference (Vol. 29).

[2] FREITAS, RA. "Advanced Automation for Space Missions [Final Report]." (1982), pp. 97-98.

[3] Geologic Map of the State of Hawai‘i, By David R. Sherrod, John M. Sinton, Sarah E. Watkins, and Kelly M. Brunt 2007, https://pubs.usgs.gov/of/2007/1089/ (09/2017)

[4] German, Randall. Sintering: from empirical observations to scientific principles, first ed., Butterworth-Heinemann, 2014. Chapter 1.

[5] K and M Krushers, Rockwell 11” drum rock crusher, https://www.kandmkrushers.com/rock-crusher-7hp-kohler-gas-gold-ore-11-drum-2-12-infeed- (01/2018)

[6] Olympus Scientific Solutions Americas Corp, Terra Portable XRD, https://www.olympus-ims.com/en/xrf-xrd/mobile-benchtop-xrd/terra/

[7] PDS Geoscience Node, Apollo Database. (08/2019), https://pds-geosciences.wustl.edu/missions/apollo/index.htm (09/2017)

[8] PDS Geoscience Node, Mars Pathfinder Database. August 2019, https://pds geosciences.wustl.edu/missions/mpf/index.htm

[9] Rhodes, John Michael, and John P. Lockwood. "Mauna Loa revealed: Structure, composition, history, and hazards." Washington DC American Geophysical Union Geophysical Monograph Series 92 (1995), pp. 241-242.

[10] Romo, Rodrigo, et al. "Planetary Lego: Designing a Construction Block from a Regolith Derived Feedstock for In Situ

Robotic Manufacturing." Earth and Space 2018: Engineering for Extreme Environments. Reston, VA: American Society of Civil Engineers, 2018. 289-296.
[11] Sanders, G. B., et al. "Use of Hawai‘i analogue sites for lunar science and in-situ resource utilization." EPSC Joint meeting 2011.
[12] Taylor, L. A., et al. "Martian meteorite Dhofar 019: A New Shergottite." Meteoritics & Planetary Science 37.8 (2002): 1107-1128.
[13] University of Arizona CheMin Database. August 2015, http://u.arizona.edu/~barbaralafuente/chemin/ (09/2019)
[14] Wagner Petrographic Thin Sections 2019. https://www.wagnerpetrographic.com/
[15] Winter, John D. Principles of igneous and metamorphic petrology, second edition. Pearson education, 2010 chapter 10.
[16] Minitti, Michelle E., et al. "Morphology, chemistry, and spectral properties of Hawaiian rock coatings and implications for Mars." Journal of Geophysical Research: Planets 112.E5 (2007).

Appendix A

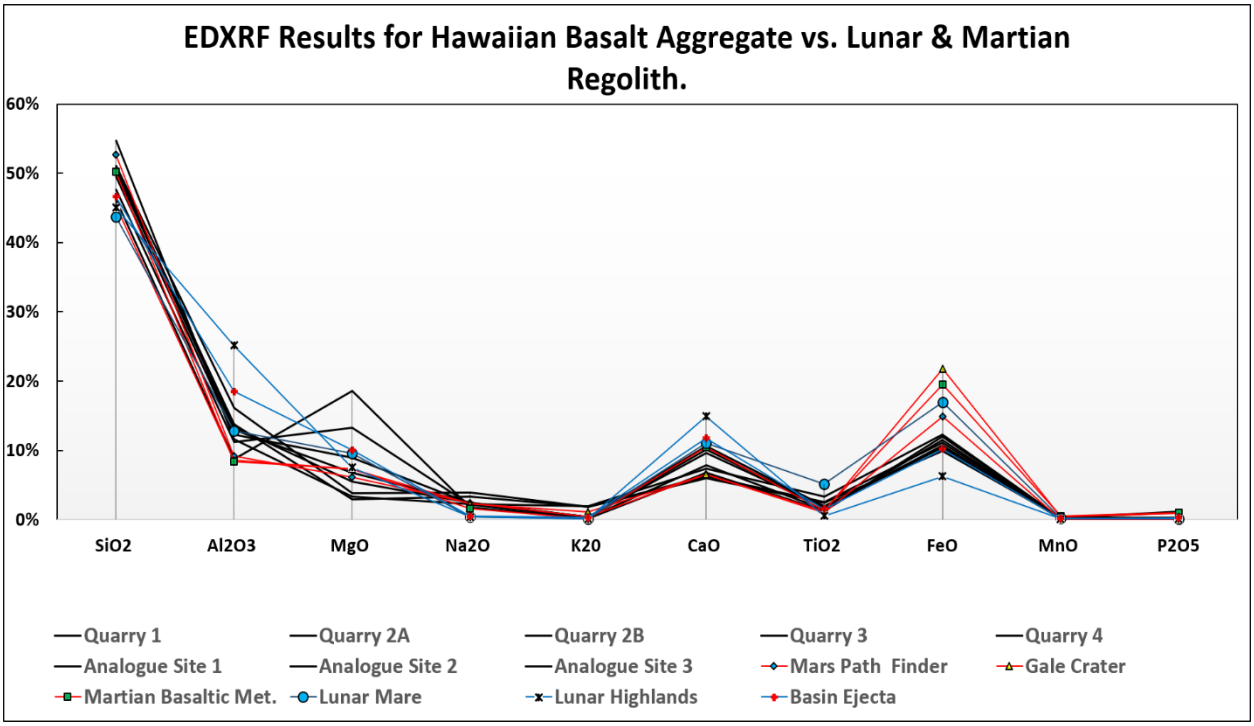

Fig. A1 EDXRF results for Hawaiian aggregate samples, displaying a spike in MgO % for samples Quarry 2B and Quarry 4. Included are EDXRF results for Martian data from the CheMin data at Gale Crater average, Mars Path Finder average and the Martian meteorite also included are Lunar data from the Apollo missions.

Source	Sample	SiO2 %	Al2O3 %	MgO %	Na2O %	K20 %	CaO %	TiO2 %	FeO %	MnO %	P2O5 %
Hawai'i	**Quarry 1**	***50.4***	***13***	***6.78***	***2.4***	***0.35***	***10.1***	***1.77***	***10.5***	***0.17***	***0.26***
Hawai'i	**Quarry 2A**	***49.5***	***12.3***	***8.89***	***2.34***	***0.34***	***9.61***	***1.71***	***10.7***	***0.16***	***0.3***
Hawai'i	**Quarry 2B**	***46.1***	***8.76***	***18.6***	***1.71***	***0.22***	***6.73***	***1.22***	***12***	***0.17***	***0.3***
Hawai'i	**Quarry 3**	***51***	***13.4***	***5.45***	***2.39***	***0.4***	***10.6***	***1.93***	***10.4***	***0.16***	***0.26***
Hawai'i	**Quarry 4**	***47.6***	***11.2***	***13.3***	***2.17***	***0.28***	***7.87***	***1.5***	***11.5***	***0.17***	***0.31***
Hawai'i	**Analogue Site 1**	***54.7***	***11.6***	***3.36***	***2.21***	***1.9***	***7.34***	***3.29***	***12.3***	***0.25***	***1.13***
Hawai'i	**Analogue Site 2**	***51.1***	***16.1***	***3.82***	***3.9***	***1.89***	***6.32***	***2.53***	***11.1***	***0.24***	***0.26***
Hawai'i	**Analogue Site 3**	***50.2***	***13.8***	***2.92***	***3.31***	***1.87***	***5.97***	***2.4***	***9.94***	***0.23***	***1.07***
MPF	**Mars Path Finder Avg.**	***52.7***	***9.218***	***6.155***	***2.373***	***0.464***	***6.527***	***1.027***	***14.86***	***0***	***0***
Earth	**Martian Meteorite**	***50.2***	***8.4***	***7.35***	***1.6***	***0.16***	***10.5***	***1.3***	***19.55***	***0.49***	***1.05***
CheMin	**Confidence Hills Pahrump**	***48.13***	***9.73***	***5.55***	***2.65***	***0.98***	***4.58***	***1.13***	***19.83***	***0.36***	***1.02***
CheMin	**John Klein Yellowknife**	***42.49***	***8.21***	***6.49***	***2.26***	***0.63***	***8.02***	***1.38***	***22.77***	***0.35***	***0.59***
CheMin	**Cumberland Yellowknife**	***41.13***	***8.63***	***9.32***	***3.01***	***0.62***	***6.66***	***0.99***	***21.95***	***0.29***	***0.86***
CheMin	**Windjana Kimberly**	***37.38***	***5.62***	***12.29***	***0.96***	***3.09***	***5.26***	***1.07***	***27.9***	***0.53***	***0.64***
CheMin	**Telegraph Peak Pahrump**	***52.7***	***10.74***	***2.93***	***3.34***	***0.98***	***4.37***	***1.23***	***18.68***	***0.22***	***1.33***
Apollo	**Lunar Mare Avg.**	***43.73***	***12.9***	***9.56***	***0.388***	***0.139***	***11.02***	***5.17***	***16.97***	***0.226***	***0.15***
Apollo	**Lunar Highlands Avg.**	***45.02***	***25.13***	***7.55***	***0.41***	***0.095***	***14.93***	***0.525***	***6.265***	***0.088***	***0.115***
Apollo	**Basin Ejecta Avg.**	***46.58***	***18.52***	***10.06***	***0.51***	***0.303***	***11.74***	***1.55***	***10.18***	***0.137***	***0.267***

Table 3 EDXRF results for all Hawaiian samples, Mars Path Finder and the Curiosity Rovers CheMin data samples from Gale Crater.

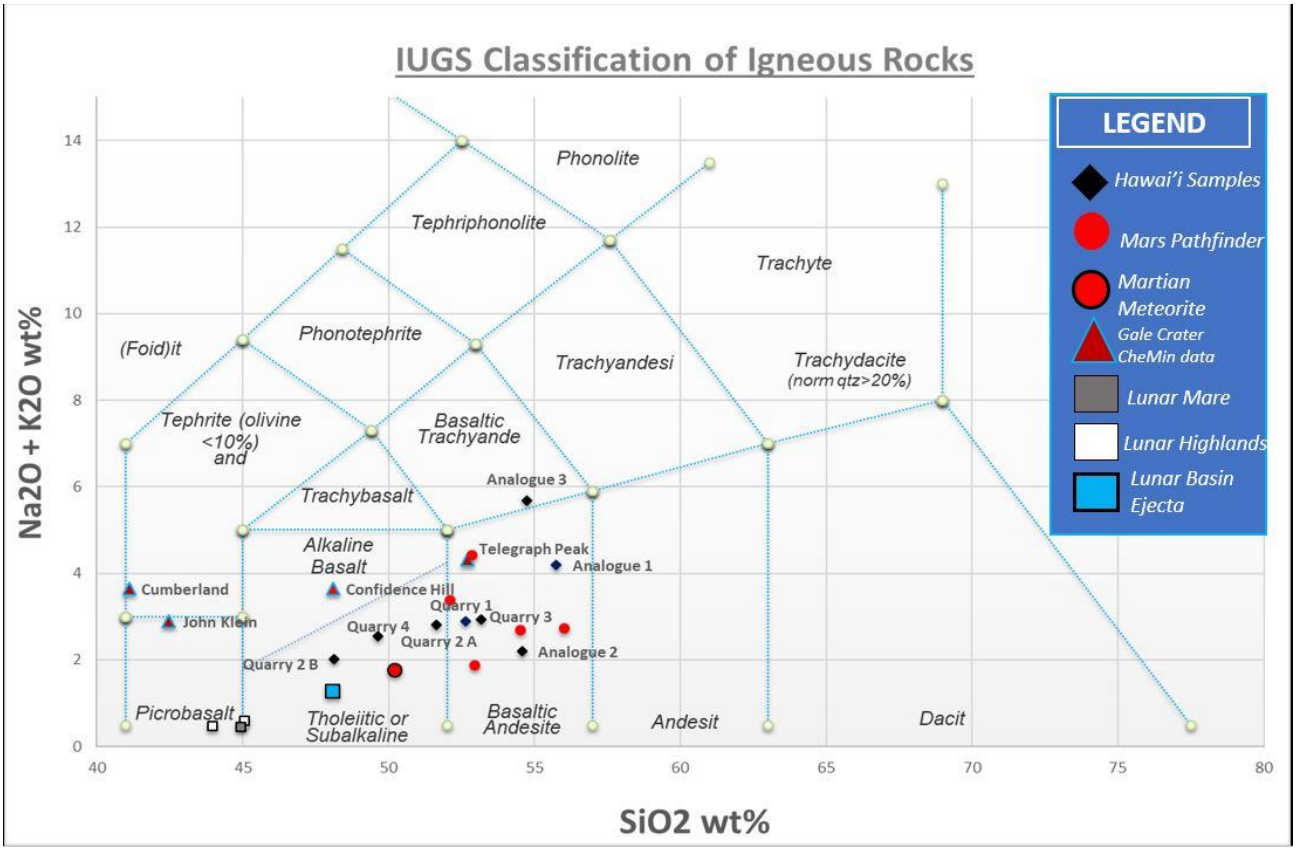

Fig. A2 IUGS Igneous Rock Classification graph for EDXRF data for all samples, Hawai'i, moon and Mars.

Quarry 1	
Mineral	%
Plagioclase	42.7
Pyroxene	24.9
Glass	16.9
Cristobalite	7.5
Formic Acid	2.5
Magnetite	2.2
Sanidine	1.8
Ilmenite	1.4
Chromite	0.2

Quarry 2 (4A)	
Mineral	%
Plagioclase	44
Pyroxene	29.8
Glass	11.6
Olivine (Fo,Fa)	4.5
Cristobalite	3.1
Magnetite	1.8
Ilmenite	1.8
Sanidine	1.6
Ulvospinel	1.5

Quarry 2 (4B)	
Mineral	%
Olivine (Fo)	33.6
Plagioclase	29.7
Pyroxene	22.3
K-Silicate	7.6
Glass	3.3
Cristobalite	1.7
Ilmenite	1.5
Chalcopyrite	0.3

Quarry 3	
Mineral	%
Plagioclase	46.4
Pyroxene	30.5
Glass	12.5
Cristobalite	4.1
Chromite	1.8
Ilmenite	1.7
Magnetite	1.2
Sanidine	0.8
Chalcopyrite	0.8
K-silicate	0.1
Sulfure	0.1

Quarry 4	
Mineral	%
Olivine (Fo)	33.6
Plagioclase	27.1
Pyroxene	24
Glass	10.7
Cristobalite	1.6
Ilmenite	1.5
Sanidine	1
Magnetite	0.4

Analogue 1	
Mineral	%
Glass	51.2
Plagioclase	37.5
Pyroxene	7.9
Ilmenite	1.5
Hematite	1.4
Cristobalite	0.4
Olivine (Fo, Fa)	0.1

Analogue 2	
Mineral	%
Glass	30.2
Plagioclase	27.4
Pyroxene	25.1
Cristobalite	7.7
Hematite	5.7
Olivine (Fo)	3.1
Ilmenite	0.4
Magnetite	0.2

Analogue 3	
Mineral	%
Plagioclase	43.9
Glass	25.6
Pyroxene	11.4
Olivine (Fo, Fa)	9
Sanidine	4.9
Chromite	3.7
Cristobalite	1.4

Fig. A3 XRD data for Hawaiian basalt aggregates

Confidence Hills	
Mineral	%
Plagioclase	38
K-feldspar	8
Olivine (Fo)	3.3
Pyroxene	21.3
Enstatite	5.4
Magnetite	6.9
Quartz	0.8
Hematite	13.4
Ilmenite	1.4
Jarosite	1.5

Cumberland	
Mineral	%
Andesine	43.6
Sanadine	3.1
Olivine (Fo)	1.8
Pyroxene	31.8
Magnetite	8.7
Anhydrite	1.6
Bassenite	1.4
Quartz	0.2
Hemetite	1.3
Ilmenite	1
Akaganeite	3.4
Halite	0.2
Pyrrhotte	1.9

Telegraph Peak	
Mineral	%
Plagioclase	38
K-feldspar	5.9
Pyroxene	11.9
Magnetite	10.9
Quartz	1.2
Cristobalite	8.7
Opal	14.5
Hematite	1.6
Ilmenite	0.9
Anhydrite	0.5
Basanite	0.5
Jarosite	2.4
Apatite	3

Windjana	
Mineral	%
Plagioclase	5.6
K-Feldspar	21.1
Olivine (Fo)	5.2
Pyroxene	46.7
Magnetite	13.8
Anhydrite	1.4
Bassenite	0.2
Quartz	0.2
Hemetite	0.9
Akaganeite	2.5
Pyrrhotite	1.3
Ilmenite	1.1

Fig. A4 XRD data for Curiosity Rover CheMin Gale Crater basalt regolith